Zinc-embedded fabrics inactivate SARS-CoV-2 and influenza A virus

Vikram Gopal[1*], Benjamin E. Nilsson-Payant[2], Hollie French[3], Jurre Y. Siegers[4], Wai-shing Yung[1], Matthew Hardwick[5], Aartjan J.W. te Velthuis[3*]

[1]Ascend Performance Materials, 1010 Travis Street, Suite 900, Houston, TX 77002, USA

[2]Department of Microbiology, Icahn School of Medicine at Mount Sinai, New York, NY 10029, USA

[3]Division of Virology, Department of Pathology, Addenbrooke's Hospital, University of Cambridge, Hills Road, CB2 2QQ, United Kingdom

[4]Department of Viroscience, Erasmus University Medical Centre, Rotterdam, the Netherlands

[5]ResInnova Laboratories, 8807 Colesville Rd, 3rd Floor, Silver Spring, MD 20910, USA

* address correspondence to: VGopal@ascendmaterials.com, ajwt6@cam.ac.uk

Key words: influenza, coronavirus, absorption, zinc, face mask

Abstract

Infections with respiratory viruses can spread via liquid droplets and aerosols, and cause diseases such as influenza and COVID-19. Face masks and other personal protective equipment (PPE) can act as barriers that prevent the spread of respiratory droplets containing these viruses. However, influenza A viruses and coronaviruses are stable for hours on various materials, which makes frequent and correct disposal of these PPE important. Metal ions embedded into PPE may inactivate respiratory viruses, but confounding factors such as absorption of viruses make measuring and optimizing the inactivation characteristics difficult. Here we used polyamide 6.6 (PA66) fibers that had zinc ions embedded during the polymerisation process and systematically investigated if these fibers can absorb and inactivate pandemic SARS-CoV-2 and influenza A virus H1N1. We find that these viruses are readily absorbed by PA66 fabrics and inactivated by zinc ions embedded into this fabric. The inactivation rate ($pfu \cdot gram^{-1} \cdot min^{-1}$) exceeds the number of active virus particles expelled by a cough and supports a wide range of viral loads. Moreover, we found that the zinc content and the virus inactivating property of the fabric remain stable over 50 standardized washes. Overall, these results provide new insight into the development of "pathogen-free" PPE and better protection against RNA virus spread.

Introduction

Infections with influenza A viruses (IAV), influenza B viruses (IBV) and coronaviruses (CoV) are a burden on our healthcare systems and economy. These respiratory RNA viruses transmit through aerosols, liquid droplets and fomites and seasonal strains typically cause a mild disease with symptoms including nasopharyngitis, fever, coughing, and headache. Nevertheless, seasonal IAV and IBV result in 290,000-645,000 deaths every year and billions of dollars in losses, in part due to increased hospitalizations and reduced work efficiencies.

The impact of highly pathogenic and pandemic IAV and CoV strains is even more severe. Over the past century, several pandemic influenza A virus (IAV) and severe acute respiratory syndrome coronaviruses (SARS-CoV) strains have infected and killed millions of people. Of particular importance were the 1918 H1N1, 1957 H2N2, and the 1968 H3N2 pandemic IAV strains, and the SARS-CoV-2 pandemic strain, the causative agent of COVID-19. These viruses can cause viral pneumonia and make it easier for secondary bacterial infections to take hold, increasing patient morbidity and mortality (1). Understanding how we can efficiently prevent the spread of these viruses will be important for current and future RNA virus outbreaks.

IAV is part of the *Orthomyxoviridae*, a family of negative-sense RNA viruses that are known for their segmented RNA genomes. The virus particle is enveloped by a double-layered membrane and contains multiple copies of the viral haemagglutinin (HA), matrix 2 (M2), and, neuraminidase (NA) proteins embedded in the membrane (2). The HA protein binds sialic acid receptors on the outside of host cells, and fuses the viral membrane and the

73 cellular plasma membrane, while the M2 protein acts as proton channel that plays a role in
74 the activation of HA and release of the viral RNA genome into the host cell. The viral RNA
75 genome consists of eight segments that are encapsidated by the viral nucleoprotein (NP)
76 and RNA polymerase as ribonucleoprotein (RNP) complexes inside virus particles (3). After
77 viral transcription, protein synthesis, replication and virion formation, the NA protein is
78 required for the release of virus particles from the host cell.
79
80 SARS-CoV-2 belongs to the *Coronaviridae*, a family of positive-sense RNA viruses that
81 infect a wide range of vertebrates, including humans (4, 5). The SARS-CoV-2 virion consists
82 of a double-layered membrane and membrane proteins spike (S), envelope (E) and matrix
83 (M). The viral RNA genome is harboured inside the virus particle and encapsidated by the
84 viral nucleocapsid protein (N). Infection of a host cell requires binding of the S protein to
85 the cellular receptor ACE2 (6). Following entry, the virus releases its viral RNA into the host
86 cell for viral protein synthesis and genome transcription and replication by the viral RNA
87 polymerase.
88
89 Various antivirals are currently available for the treatment of influenza and CoV infections,
90 including RNA polymerase inhibitors favipiravir and remdesivir (7-9). In addition, vaccines
91 are available or in development that target the HA or S protein to prevent infection and
92 spread of IAV and SARS-CoV-2 (10). Unfortunately, vaccines are not readily available for
93 emerging RNA viruses, and existing RNA viruses can become resistant against antivirals
94 and escape immune pressures due to their relatively high mutation rate (11, 12). Use of
95 personal protective equipment (PPE), such as face masks, is therefore recommended by
96 health organizations to prevent respiratory virus spread and several studies have supported

97 their efficacy (13-15). However, opponents of the use of face masks have pointed to
98 complicating factors, including observations that respiratory viruses are stable for days to
99 hours on fabrics and that N95 respirators require careful decontamination to allow their re-
100 use (16-19). Further considerations are the additional environmental waste that disposable
101 face masks produce, the poor fit of some masks, and the potential health hazard that
102 discarded masks present (20, 21). Development of PPE that can trap and inactivate
103 respiratory viruses may help address some of these concerns or simplify their use in day-to-
104 day life.
105
106 Previous research has shown that IAVs and CoVs can be inactivated by metal surfaces, such
107 as copper and zinc (22-24). While the exact underlying inactivation mechanisms are not
108 fully understood, evidence suggests that metal ions can induce RNA hydrolysis, membrane
109 destabilisation, or viral protein inactivation or degradation (25-27). So far, few studies have
110 investigated if metal ions embedded in fabrics can inactivate RNA viruses, in part because
111 absorbance and fabric density differences among fabrics present confounding factors that
112 the protocols approved for testing the inactivating properties of surfaces do not account
113 for.
114
115 To tackle some of these confounding issues, we here measured the ability of different
116 fabrics, such as cotton, polyamide 6.6 (PA66) and polypropylene (PPP), to trap H1N1 IAV
117 and pandemic SARS-CoV-2, and we explore how we can remove these viruses from the
118 fabrics to test for inactivation. We find that cotton and PA66 readily absorb respiratory
119 viruses, and that zinc ions embedded in PA66-based fabrics resulted in approximately a 2-
120 log reduction in virus titer, which is more than sufficient to inactivate the number of

121 infectious IAV virus particles (~24 plaque forming units [pfu]) present in a cough (28). Virus
122 inactivation plateaued over time. Overall, these results provide new insight into the
123 protective properties of fabrics used for face masks and the development of "pathogen-
124 free" fabrics.
125
126
127 ## Results
128 **Influenza virus absorbance by cotton, polypropylene and polyamide**
129 Various studies have investigated the filtration properties of fabrics and have investigated
130 factors such as breathability, hydrophobicity and/or electrostaticity. Fabrics also have a
131 different weight per square meter (gram/m^2) and different moisture retention abilities, with
132 cotton absorbing up to 500% of its weight and PA66 absorbing as little as 0.3% of its
133 weight, depending on environmental conditions (29). These different properties may affect
134 how fabrics trap and/or release aerosols or liquid droplets containing RNA viruses. For
135 instance, PPE with poor absorbing properties that become contaminated with viruses may
136 retain these viruses on their surface thus become a potential health hazard if not disposed
137 of properly. Presently, it is not fully understood how moisture retention is correlated with
138 virus particle absorption. To investigate this relationship, we added IAV strain A/WSN/33
139 (H1N1) to International Antimicrobial Council (IAC) issued cotton, a textile PA66 fabric, or
140 PPP from a disposable type II 3-ply face mask (Fig. 1A). After a 30-min incubation at room
141 temperature, the fabrics were washed with PBS to remove unabsorbed virus (Fig. 1B). To
142 estimate the amount of remaining liquid on each fabric, each sample tube with fabric was
143 weighed and compared to its dry weight. As shown in Fig. 1C and D, cotton and PA66
144 retained more liquid than PPP, both relative to the applied volume and the weight of the

145 fabric. Subsequent analysis of the IAV titer in the input and fabric washes showed that the
146 cotton and woven PA66 fabrics readily absorbed the applied virus, while less virus was
147 observed by the PPP fabric (Fig. 1E, F), which is in line with the hydrophobicity of PPP (30).
148

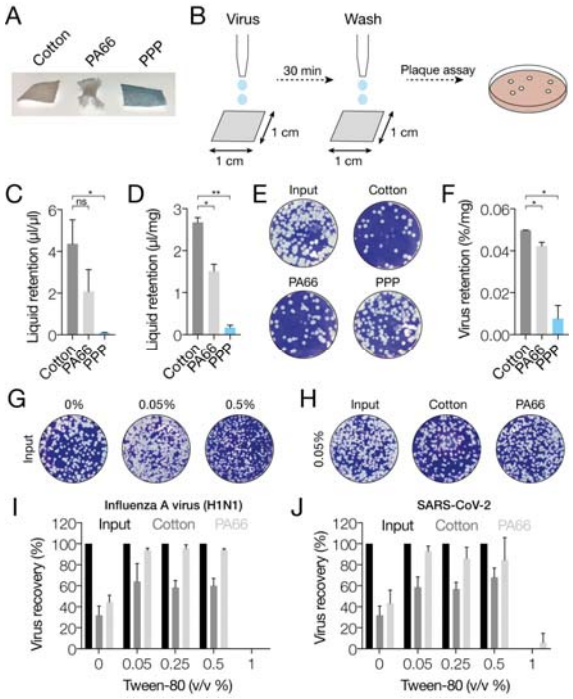

149

150 **Figure 1. Absorption and release of IAV and SARS-CoV-2 from fabrics**. **A**) Photographs of cotton
151 control, PA66 and polypropylene fabric samples. **B**) Schematic of experimental procedure for exposing
152 and isolating RNA virus from fabrics. **C**) Analysis of virus medium retention by fabrics per volume of
153 input medium. Values were obtained by weighing each fabric before and after addition of virus medium,
154 and after removal of the virus medium. **D**) Analysis of virus medium retention by fabrics normalized by
155 dry weight of each fabric. Values were obtained by weighing each fabric before and after addition of
156 virus medium, and after removal of the virus medium. **E**) Plaque assay of IAV present in virus medium
157 after removal of the medium from each fabric. **F**) Quantitation of the amount of virus remaining on each
158 fabric, normalized by the dry weight of each fabric. **G**) Effect of different tween-80 concentrations on
159 IAV plaque assay read-out. **H**) Effect of 0.05% tween-80 in PBS on the amount of virus released from
160 each fabric. **I**) Quantitation of IAV titers after absorption of the virus to the fabrics and washing of the

161 fabrics with PBS or PBS containing different concentrations of tween-80. **J**) Quantitation of SARS-CoV-2
162 titers after absorption of the virus to the fabrics and washing of the fabrics with PBS or PBS containing
163 different concentrations of tween-80. Error bars indicate standard deviation. Asterisk indicates p-value,
164 with * $p<0.05$, ** $p<0.005$, and ns $p>0.05$.
165
166
167 In order to remove IAV from the cotton and PA66 fabrics without inactivating the virus, we
168 added different concentrations of polysorbate-80 (tween-80) - a mild detergent that is also
169 used in IAV vaccine preparations - to the PBS wash buffer (Fig. 1G). We did not observe any
170 cytopathic effects of the detergent on the Madin-Darby Canine Kidney (MDCK) cells used
171 for the plaque assay, but did find that the presence of 0.05%-0.1% tween-80 increased the
172 apparent viral titer relative to infections in PBS (Fig. 1G), whereas 0.25-0.5% tween-80
173 reduced the apparent IAV plaque size (Fig. 1G). We found that 0.05% tween-80 succeeded
174 in recovering more than 94% of the virus from the PA66 woven fabric, whereas 61% was
175 removed from the cotton fabric (Fig. 1H and I). Higher concentrations, such as 1% tween-
176 80, prevented IAV infection (Fig. 1I).
177
178 To confirm whether other viruses can be removed from cotton and woven PA66 as well, we
179 repeated the experiment with SARS-CoV-2. We found that over 92% of SARS-CoV-2 can be
180 recovered from the woven PA66 fabric using 0.05% tween-80, while up to 59% could be
181 recovered from the cotton fabric (Fig. 1J). Together, these results demonstrate that IAV
182 and SARS-CoV-2 are strongly absorbed by cotton and PA66, suggesting that these
183 materials would trap respiratory viruses inside face masks. At the same time, these findings
184 imply that PPP is poor at trapping respiratory viruses. Since IAV and SARS-CoV-2 can be

185 removed from a PA66 fabric with a mild detergent, this protocol can be useful for testing
186 the inactivating properties of fabrics.
187
188
189 **Influenza virus is inactivated by zinc ions**
190 Copper and zinc surfaces or particles can inactivate IAV strains and seasonal CoV HCoV-
191 229E, and PPP imbued with copper oxide can potentially inactivate IAV (22, 25, 26, 31). For
192 embedding into polymers, zinc ions provide benefits over copper ions as zinc has a much
193 higher propensity to ionize than copper, and thereby provides a much faster reaction
194 potential. Moreover, zinc oxide, which we embedded in the PA66 polymer used here, is
195 considered a Generally regarded as Safe (GRAS) compound by the FDA, which can speed
196 up the development process. Finally, zinc does not cause discolouration of the polymer or
197 fabric enabling a broader applicability. However, like copper, zinc ions are cytotoxic in
198 tissue culture (Fig. 2A), which confounds analysis of their effect on viral titers. We found
199 that addition of an equimolar concentration of EDTA following the virus incubation with
200 zinc ions (Fig. 2B) can efficiently chelate zinc ions and prevent cytotoxic effects (Fig. 2C).
201 EDTA alone does not have any cytotoxic effects and does not reduce viral titers (Fig. 2A).
202
203

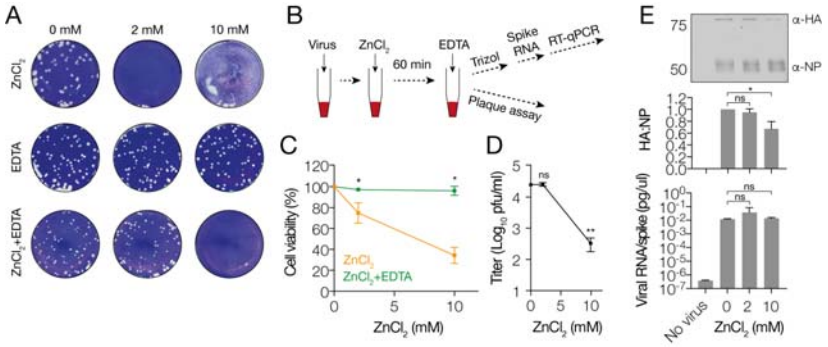

204 **Figure 2. IAV is inactivated by zinc ions**. **A**) Plaque assay showing the effect of different zinc chloride
205 and EDTA concentrations on IAV titers. **B**) Experimental approach for inactivating IAV with zinc ions and
206 neutralization of zinc ions using EDTA. **C**) Cytotoxicity analysis of zinc chloride and EDTA in MDCK cells.
207 **D**) IAV titers after exposure to zinc chloride and neutralization with EDTA as measured on MDCK cells. **E**)
208 Western blot IAV HA and NP protein levels after exposure to zinc chloride and neutralization with EDTA.
209 Upper panel shows quantitation of western signal and middle panel the western signal as detected with
210 LI-COR. Bottom panel shows NA segment RT-qPCR analysis of IAV virus after exposure to zinc chloride
211 and neutralization with EDTA. Error bars represent standard deviation. Asterisk indicates p-value, with *
212 $p<0.05$, ** $p<0.005$, and ns $p>0.05$.
213

214 To investigate if zinc ions can directly inactivate IAV, we incubated influenza virus with
215 varying concentrations of zinc chloride. After 60 min, the reactions were stopped with an
216 equimolar amount of EDTA and subsequently diluted for virus titer determination by
217 plaque assay (Fig. 2B). As shown in Fig. 2D, we found that addition of zinc chloride resulted
218 in a significant reduction in the IAV titer. Previous research has shown that metal ions can
219 destabilize viral proteins (25). To gain more insight into the mechanism of virus
220 inactivation, viral protein levels in the zinc chloride-treated samples were analysed by
221 western blot. As shown in Fig. 2E, we found that in the presence of zinc chloride, HA levels
222 were reduced in a concentration-dependent manner, while NP levels did not diminish (Fig.
223 2E). This result thus suggest that zinc ions may affect the IAV surface proteins more
224 significantly than the internal proteins. To test if IAV RNA levels were affected, we added a
225 120-nucleotide long spike RNA to each sample, extracted viral RNA, and performed reverse
226 transcriptions (RT) using a 3′ terminal NA primer. cDNA levels were next quantified using
227 quantitative polymerase chain reaction (qPCR) of the NA gene-encoding segment and
228 normalized to the spike RNA level (Fig. 2E). No effect of zinc chloride on viral NA segment

229 levels was found. Together, these results imply that zinc ions can inactivate an IAV (H1N1)
230 strain by destabilization of the viral surface proteins.
231
232
233 **Influenza and coronavirus strains are inactivated on fabrics containing zinc ions**
234 The above results suggest that zinc ions can directly inactivate an IAV H1N1 strain. To
235 investigate if these inactivating properties are also present when zinc ions are embedded in
236 a PA66 matrix, we used 0.4 gram of a textile PA66 fabric containing 328 ppm zinc ions
237 (equivalent to 2.5 mM; abbreviated as KF1). Incubation of KF1 with virus and washing of the
238 fabrics using a PBS buffer containing 0.05% tween-80 and 10 mM EDTA (PBSTE; Fig. 3A),
239 resulted in an approximately 2-log reduction of the IAV and SARS-CoV-2 titers compared to
240 a PA66 control fabric after 1 h (Fig. 3B and C). To confirm that inactivation of these viruses
241 occurred on KF1, viral protein levels were analysed in the PBSTE wash eluate by western
242 blot (Fig. 3D and E). Any virus that remained in the fabric after extraction with PBSTE, was
243 lysed and extracted using Trizol and analyzed by western blot as well. Western blots
244 showed a reduction in the HA and S protein level in the virus eluate that was removed from
245 the KF1 fabric compared to the control fabric eluate for IAV and SARS-CoV-2, respectively
246 (Fig. 3D and E). The signal obtained from the virus that remained on each fabric after the
247 PBSTE extraction was close to background, in line with the observations in Fig. 1, and we
248 were only able to quantify the SARS-CoV-2 signal, but observed no statistically significant
249 difference. Overall, we conclude that inactivation of IAV and SARS-CoV-2 occurs on a fabric
250 embedded with zinc oxide, analogous to the previously observed effects of copper oxide
251 (31). To better investigate the rate of reduction, we incubated KF1 with virus for different
252 lengths of time and subtracted the absorbed virus titer in the negative control from the

253 level of reduction in the KF1 fabric and fitted the data with a logarithmic equation (Fig. 3F).

254 A maximum reduction occurred between 30 seconds and 5 min of incubation, and the virus

255 titer reduction reached a plateau after approximately 50 min.

256

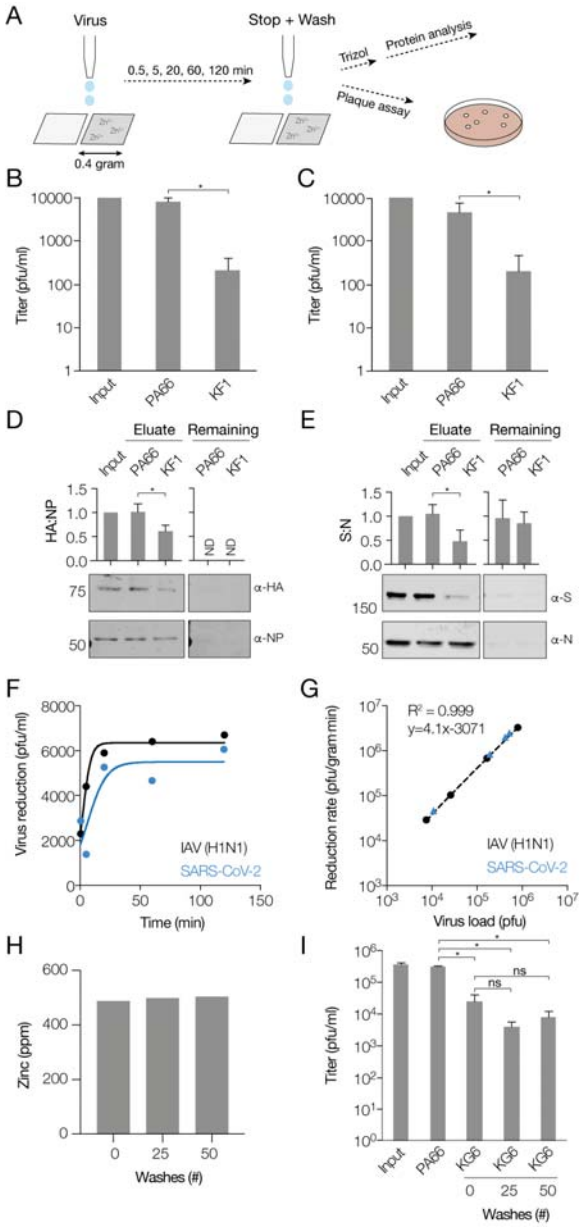

257

258 **Figure 3. Inactivation of IAV and SARS-CoV-2 on fabrics**. **A**) Schematic of testing procedure for fabrics

259 without or with embedded zinc oxide. **B**) IAV titer in input, or PA66 control or KF1 fabric eluates. **C**)

260 SARS-CoV-2 titer in input, or PA66 control or KF1 fabric eluates. One representative experiment is

261 shown. **D**) Western blot analysis of IAV HA and NP protein levels after exposure of IAV to the KF1 or
262 control fabric. Both the virus that was removed (eluate) from each fabric with PBSTE as well as the virus
263 that remained on each fabric was analyzed. **E**) Western blot analysis of SARS-CoV-2 S and N protein
264 levels after exposure of virus to the KF1 or control fabric. Both the virus that was removed (eluate) from
265 each fabric with PBSTE as well as the virus that remained on each fabric was analyzed. **F**) Time course of
266 IAV or SARS-CoV-2 titer reduction by the KF1 fabric minus the titer reduction by the PA66 control
267 without embedded zinc. One representative time course is shown. Data were fit with logarithmic
268 equation. **G**) Reduction rate of IAV or SARS-CoV-2 titer after exposure to KF1 fabric. Data points were
269 obtained by from time courses experiments in which we varied the viral load and subsequently
270 estimated the maximum reduction rate (exponential phase) for each time course. Reduction was
271 normalized to $pfu \cdot gram^{-1} \cdot min^{-1}$ using the dry fabric weight. IAV and SARS-CoV-2 data points were fit
272 with a linear line and no difference was observed between the two fits. R^2 for IAV fit is shown. **H**) Zinc
273 content in KG6 fabric after repeated washing according to the standardized home laundry test protocol
274 AATCC M6-2016. One representative experiment for one batch of fabric is shown. **I**) Reduction rate of
275 IAV titer after exposure to unwashed or washed KG6 fabric. Error bars represent standard deviation.
276 Asterisk indicates p-value, with * $p<0.05$ and ns $p>0.05$.
277
278
279 **Inactivation of IAV and coronaviruses scales with virus load**
280 To investigate the robustness and saturation level of the inactivation by fabrics containing
281 embedded zinc oxide, we next performed experiments with KF1 and varied the viral load
282 added to each fabric over a range of 10^3 to 10^7 pfu. The liquid volume applied to each fabric
283 was kept constant. After incubation for different periods of time, fabrics were washed with
284 PBSTE, virus titers estimated by plaque assay and the virus titer reduction rate calculated
285 based on the shortest incubation time. Reduction rates were subsequently normalized by
286 the dry weight of each fabric. As shown in Fig. 3G, the rate of reduction in virus titer (in

287 pfu·gram^{-1}·min^{-1}) scaled with virus load. On a log-log plot, the data could be fit with a linear
288 equation. To confirm the robustness of these findings, we performed the same
289 experiments with SARS-CoV-2, and found a similar behavior (Fig. 3H).

290 To investigate if fabrics constructed from fibers containing zinc ions maintain their
291 zinc oxide content after washing, a KF1 fabric with 500 ppm zinc ions (equivalent to 5.3 mM;
292 internal code KG6) was washed 25 or 50 times using the standardized home laundry test
293 protocol AATCC M6-2016. Subsequent analysis of the zinc content after washing revealed
294 that the zinc content remained relatively constant in the PA66 fabrics for up to 50 washes
295 (Fig. 3H). We next confirmed if these washed fabrics were still able to reduce virus titers and
296 incubated 0.4 g of unwashed or washed fabric with a fixed amount of IAV and removed
297 inactivated virus with PBSTE. Analysis of the virus titers showed that both washed fabrics
298 were able reduce the IAV titer by approximately 2-logs (Fig. 3I). Overall, these results
299 suggest that the PA66 fabric containing zinc can inactivate both IAV and SARS-CoV-2 and
300 that this property is retained after 50 washes.

301

302 **Discussion**

303 Infections with respiratory RNA viruses cause regular seasonal epidemics and occasional
304 pandemics, and thus present a severe burden on our personal health, healthcare systems,
305 and economy. While seasonal respiratory viruses - including over 160 different rhinoviruses,
306 human CoVs strains NL63, OC43, HKU1 and 229E, influenza A, B and C viruses, human
307 respiratory syncytial virus, human parainfluenza viruses, and human metapneumovirus –
308 typically cause mild disease, IAV and CoVs have also been associated with zoonotic
309 outbreaks and lethal pandemics. Vaccines and antivirals are available or in development for
310 various respiratory viruses, but the appearance of resistance to antivirals or vaccines is a

311 known or potential problem. In the absence of new vaccines or antivirals, one way to fight
312 RNA viruses is to limit respiratory virus spread through efficient PPE.
313
314 To better understand how respiratory RNA viruses are absorbed and inactivated on fabrics,
315 we here added IAV and SARS-CoV-2 to cotton, PA66, and PPP. We find strong absorption
316 by cotton and PA66 in the standard laboratory buffer PBS, and that addition of tween-80
317 results in efficient virus release from PA66, but not from cotton. A previous clinical trial
318 found that cotton masks with strong absorbing properties may be associated with a higher
319 risk of infection when reused and our finding that cotton does not release IAV or SARS-
320 CoV-2 efficiently after washing is in line with this observation (16). By contrast, virus
321 retention on PPP, which is used for the construction of disposable 3-ply masks, is poor, in
322 line with its hydrophobic properties (30). This result implies that respiratory viruses remain
323 on the surface of these masks and together with findings that SARS-CoV-2 can survive on
324 various surfaces for several hours to days, and even 7 days on PPP-based surgical face
325 masks (19, 32), PPP-based masks may increase the risk of infection if not handled and
326 disposed of properly. However, PPP has of course alternative properties, such as good
327 breathability, filtration, and electrostatic properties and will thus has a purpose in the right
328 situation.
329
330 The use of any face mask or other PPE, even if used temporarily but correctly to prevent
331 spread, is better than wearing no face mask as it may reduce the risk of infection with
332 respiratory viruses (13-15). However, the above considerations suggest that there is a
333 potential for the use of pathogen-inactivating PPE, i.e. fabrics that can both absorb as well
334 as inactivate viruses. In particular the use of zinc and copper ions in PPE is promising in this

335 regard, as these metals can inactivate IAV and SARS-CoV-2 (Fig. 2, 3) (22, 24, 26). Using a
336 PA66-based fabric from which we could easily remove absorbed virus with a mild detergent
337 (Fig. 1), we tested the effect of zinc ions embedded in a matrix on the infectiousness of IAV
338 and pandemic SARS-CoV-2. We consistently found a rapid reduction in the titer of all
339 viruses tested and at viral loads that far exceed the number of infectious IAV particles
340 present in a cough (Fig. 3). After washing the fabrics using a standardized protocol, both
341 the zinc content as well as the inactivating properties of the PA66 fabric were retained,
342 suggesting that this fabric is reusable at least 50 times. This property may be of particular
343 importance for designing reusable PPE that could help reduce environmental waste, virus
344 transmission, and costs.
345
346 We also investigated the mechanism by which zinc ions inactivate IAV and SARS-CoV-2.
347 RT-qPCR analysis showed no significant reduction in viral RNA integrity after treatment
348 with zinc ions. By contrast, analysis of the stability of the viral surface and capsid proteins
349 revealed a reduced stability of the virus surface proteins HA and S, for IAV and SARS-CoV-
350 2, respectively, after exposure to zinc ions, while no effect on the internal nucleoprotein or
351 nucleocapsid proteins was detected. We observed a similar altered surface protein to
352 nucleoprotein ratio after exposure to the zinc containing PA66 fabric KF1. Together, these
353 results suggest that the reduction in virus titer after exposure to zinc ions derives from
354 inactivation of the viral surface proteins. This is in line with previous research using copper
355 ions (25). Research has shown that zinc and copper ions can also induce oxidative reactions,
356 inactivation of the viral proton channels, or viral membrane destabilization and we cannot
357 exclude that these processes may play a role in the inactivation as well (27, 33, 34).
358

359 Overall, these results strongly suggest that virus inactivating fabrics can offer enhanced
360 safety over widely used cotton and PPP-based PPE. Our findings may therefore be
361 important for health care workers who are exposed to infected patients for prolonged
362 periods, people with underlying risk factors needing additional protection, and people who
363 need to frequently remove their PPE.
364
365
366 ## Methods
367
368 **Influenza viruses and cells**
369 MDCK cells were originally sources from ATCC. Influenza A/WSN/33 (H1N1) virus was
370 rescues from plasmids (35) and grown on MDCK cells in Minimal Essential Medium (MEM)
371 containing 0.5% foetal bovine serum (FBS) at 37 °C and 5% CO_2. Plaque assays were
372 performed on 100% confluent MDCK cells in MEM containing 0.5% FBS with a 1% agarose
373 overlay. Ten-fold virus dilutions were grown under a 1% agarose in MEM containing 0.5%
374 FBS overlay for 2 days at 37 °C. Cell viability was measured using a CellTiter Blue assay
375 (Promega).
376
377 **Coronaviruses and cells**
378 SARS-CoV-2 (Bavpat-1 and USA-WA1/2020) were grown on African Green Monkey kidney
379 epithelial Vero-E6 cells in Dulbecco's Minimal Essential Medium (DMEM) supplemented
380 with 10% FBS. For plaque assay analysis, Vero-E6 cells were seeded in 12-well plates and
381 infected at 100% confluency. Ten-fold virus dilutions were grown under a 1% agarose

382 overlay in DMEM containing 0.5% FBS for 2 days at 37 °C. Experiments were performed in a
383 BSL3 lab according to approved biosafety standards.
384
385 **Fabrics**
386 Fabric samples were cut by cleaned scissors. The cotton fabric was issued and certified by
387 the IAC (lot number IACVC01012020). The PA66 fabrics with zinc ions (Microban Additive
388 Z07; EPA Reg. No. 42182-8) and a control fabric without zinc ions were produced and
389 provided by Ascend Performance Materials. The PPP disposable type II 3-ply face mask
390 (Medical Products Co, Ltd) was BS EN14638:2019 type II compliant. PA66 fabrics were
391 washed according to the standardized home laundry test protocol AATCC M6-2016.
392 Inductively coupled plasma (ICP) analysis was used to determine the zinc content after
393 fabric washing.
394
395 **Virus absorption and extraction**
396 To test the ability of fabrics to reduce viral titres, we used a modified ISO 18184 protocol.
397 Briefly, 100 µl of IAV strain A/WSN/33 (H1N1) was applied in 5-10 µl droplets to cotton, a
398 textile PA66 fabric, or PPP cut from medical grade face masks. The size of the fabrics varied
399 from 1 cm^2 to 0.4 gram, as indicated in the figures. After an incubation at room
400 temperature as indicated, the fabrics were washed with PBS, PBS containing tween-80, or
401 PBS containing 0.05% tween-80 and 10 mM EDTA through vortexing. After virus removal, 1
402 ml of Trizol (Invitrogen) was added to each fabric to extract remaining viral protein and
403 RNA. Experiments were performed in triplicate, unless noted otherwise. Data was analysed
404 in Graphpad Prism 8 using 1-way ANOVA.
405

RT-qPCR and western blot

RNA extraction from Trizol was performed as described previously(36), while protein was extracted from the interphase using isopropanol precipitation(37). Precipitated protein was washed in ethanol, resuspended in 5x SDS-PAGE loading buffer, sonicated for 10 seconds, and boiled for 10 min before 8% SDS-PAGE analysis. Western blot was performed using antibodies directed against IAV HA (Invitrogen, PA5-34929) and NP (GeneTex, GTX125989) and SARS-CoV-2 S (Abcam ab272504) and N (GeneTex, GTX632269). Membranes were washed in TBS containing 0.1% tween-20. Spike RNA was purchased from IDT and had the sequence 5′-AGUAGAAACAAGGCGGUAGGCGCUGUCCUUUAUCCAGACAACCAUUACCUGUCCACACAAUCUGCCCUUUCGAAAGAUCCCAACGAAAAGAGAGACCACAUGGUCCUUCCUGCUUUUGCU-3′. Isolated RNA was reverse transcribed using SuperScript III and a primer binding to the 3′ end of the NA segment (36). qPCR was performed as described previously (36). Data was analysed in Graphpad Prism 8 using one-way ANOVA with multiple corrections.

Acknowledgments

We thank Shanaka Rodrigo, Natasha Virjee, Chris Hsiung, and Benjamin Tenoever for helpful discussions, materials and information. AtV is supported by joint Wellcome Trust and Royal Society grant 206579/Z/17/Z and the National Institutes of Health grant R21AI147172.

Competing interests

This study was funded in part by Ascend Performance Materials. VG and W-sY are employed by Ascend Performance Materials. MH is employed by ResInnova and hired by Ascend Performance Materials to perform experiments and analyze the data. Icahn School of Medicine at Mount Sinai and University of Cambridge received consultancy fees from Ascend Performance Materials for experimental work and data analysis.

References

1. McCullers JA. 2014. The co-pathogenesis of influenza viruses with bacteria in the lung. Nat Rev Microbiol 12:252-62.
2. Hutchinson EC, Charles PD, Hester SS, Thomas B, Trudgian D, Martinez-Alonso M, Fodor E. 2014. Conserved and host-specific features of influenza virion architecture. Nat Commun 5:4816.
3. Te Velthuis AJ, Fodor E. 2016. Influenza virus RNA polymerase: insights into the mechanisms of viral RNA synthesis. Nat Rev Microbiol 14:479-93.
4. Zhu N, Zhang D, Wang W, Li X, Yang B, Song J, Zhao X, Huang B, Shi W, Lu R, Niu P, Zhan F, Ma X, Wang D, Xu W, Wu G, Gao GF, Tan W, China Novel Coronavirus I, Research T. 2020. A Novel Coronavirus from Patients with Pneumonia in China, 2019. N Engl J Med 382:727-733.
5. Coronaviridae Study Group of the International Committee on Taxonomy of V. 2020. The species Severe acute respiratory syndrome-related coronavirus: classifying 2019-nCoV and naming it SARS-CoV-2. Nat Microbiol 5:536-544.

452 6. Letko M, Marzi A, Munster V. 2020. Functional assessment of cell entry and receptor
453 usage for SARS-CoV-2 and other lineage B betacoronaviruses. Nat Microbiol 5:562-
454 569.
455 7. Goldhill DH, Te Velthuis AJW, Fletcher RA, Langat P, Zambon M, Lackenby A, Barclay
456 WS. 2018. The mechanism of resistance to favipiravir in influenza. Proc Natl Acad Sci
457 U S A 115:11613-11618.
458 8. Pruijssers AJ, George AS, Schafer A, Leist SR, Gralinksi LE, Dinnon KH, 3rd, Yount BL,
459 Agostini ML, Stevens LJ, Chappell JD, Lu X, Hughes TM, Gully K, Martinez DR, Brown
460 AJ, Graham RL, Perry JK, Du Pont V, Pitts J, Ma B, Babusis D, Murakami E, Feng JY,
461 Bilello JP, Porter DP, Cihlar T, Baric RS, Denison MR, Sheahan TP. 2020. Remdesivir
462 Inhibits SARS-CoV-2 in Human Lung Cells and Chimeric SARS-CoV Expressing the
463 SARS-CoV-2 RNA Polymerase in Mice. Cell Rep 32:107940.
464 9. Williamson BN, Feldmann F, Schwarz B, Meade-White K, Porter DP, Schulz J, van
465 Doremalen N, Leighton I, Yinda CK, Perez-Perez L, Okumura A, Lovaglio J, Hanley PW,
466 Saturday G, Bosio CM, Anzick S, Barbian K, Cihlar T, Martens C, Scott DP, Munster VJ,
467 de Wit E. 2020. Clinical benefit of remdesivir in rhesus macaques infected with SARS-
468 CoV-2. Nature 585:273-276.
469 10. van Riel D, de Wit E. 2020. Next-generation vaccine platforms for COVID-19. Nat
470 Mater 19:810-812.
471 11. Eckerle LD, Becker MM, Halpin RA, Li K, Venter E, Lu X, Scherbakova S, Graham RL,
472 Baric RS, Stockwell TB, Spiro DJ, Denison MR. 2010. Infidelity of SARS-CoV Nsp14-
473 exonuclease mutant virus replication is revealed by complete genome sequencing.
474 PLoS Pathog 6:e1000896.

475 12. Cheung PP, Rogozin IB, Choy KT, Ng HY, Peiris JS, Yen HL. 2015. Comparative
476 mutational analyses of influenza A viruses. RNA 21:36-47.
477 13. Gandhi M, Beyrer C, Goosby E. 2020. Masks Do More Than Protect Others During
478 COVID-19: Reducing the Inoculum of SARS-CoV-2 to Protect the Wearer. J Gen Intern
479 Med doi:10.1007/s11606-020-06067-8.
480 14. Jefferson T, Del Mar CB, Dooley L, Ferroni E, Al-Ansary LA, Bawazeer GA, van Driel
481 ML, Nair S, Jones MA, Thorning S, Conly JM. 2011. Physical interventions to interrupt
482 or reduce the spread of respiratory viruses. Cochrane Database Syst Rev
483 doi:10.1002/14651858.CD006207.pub4:CD006207.
484 15. Wu J, Xu F, Zhou W, Feikin DR, Lin CY, He X, Zhu Z, Liang W, Chin DP, Schuchat A.
485 2004. Risk factors for SARS among persons without known contact with SARS
486 patients, Beijing, China. Emerg Infect Dis 10:210-6.
487 16. MacIntyre CR, Seale H, Dung TC, Hien NT, Nga PT, Chughtai AA, Rahman B, Dwyer
488 DE, Wang Q. 2015. A cluster randomised trial of cloth masks compared with medical
489 masks in healthcare workers. BMJ Open 5:e006577.
490 17. Wang Y, Tian H, Zhang L, Zhang M, Guo D, Wu W, Zhang X, Kan GL, Jia L, Huo D, Liu B,
491 Wang X, Sun Y, Wang Q, Yang P, MacIntyre CR. 2020. Reduction of secondary
492 transmission of SARS-CoV-2 in households by face mask use, disinfection and social
493 distancing: a cohort study in Beijing, China. BMJ Glob Health 5.
494 18. Fischer RJ, Morris DH, van Doremalen N, Sarchette S, Matson MJ, Bushmaker T,
495 Yinda CK, Seifert SN, Gamble A, Williamson BN, Judson SD, de Wit E, Lloyd-Smith JO,
496 Munster VJ. 2020. Effectiveness of N95 Respirator Decontamination and Reuse
497 against SARS-CoV-2 Virus. Emerg Infect Dis 26.

498 19. Chin AWH, Chu JTS, Perera MRA, Hui KPY, Yen HL, Chan MCW, Peiris M, Poon LLM.
499 2020. Stability of SARS-CoV-2 in different environmental conditions. Lancet Microbe
500 1:e10.
501 20. Prata JC, Silva ALP, Walker TR, Duarte AC, Rocha-Santos T. 2020. COVID-19 Pandemic
502 Repercussions on the Use and Management of Plastics. Environ Sci Technol 54:7760-
503 7765.
504 21. Adyel TM. 2020. Accumulation of plastic waste during COVID-19. Science 369:1314-
505 1315.
506 22. Noyce JO, Michels H, Keevil CW. 2007. Inactivation of influenza A virus on copper
507 versus stainless steel surfaces. Appl Environ Microbiol 73:2748-50.
508 23. Biryukov J, Boydston JA, Dunning RA, Yeager JJ, Wood S, Reese AL, Ferris A, Miller D,
509 Weaver W, Zeitouni NE, Phillips A, Freeburger D, Hooper I, Ratnesar-Shumate S,
510 Yolitz J, Krause M, Williams G, Dawson DG, Herzog A, Dabisch P, Wahl V, Hevey MC,
511 Altamura LA. 2020. Increasing Temperature and Relative Humidity Accelerates
512 Inactivation of SARS-CoV-2 on Surfaces. mSphere 5.
513 24. Warnes SL, Little ZR, Keevil CW. 2015. Human Coronavirus 229E Remains Infectious
514 on Common Touch Surface Materials. mBio 6:e01697-15.
515 25. Fujimori Y, Sato T, Hayata T, Nagao T, Nakayama M, Nakayama T, Sugamata R, Suzuki
516 K. 2012. Novel antiviral characteristics of nanosized copper(I) iodide particles
517 showing inactivation activity against 2009 pandemic H1N1 influenza virus. Appl
518 Environ Microbiol 78:951-5.
519 26. Imai K, Ogawa H, Bui VN, Inoue H, Fukuda J, Ohba M, Yamamoto Y, Nakamura K.
520 2012. Inactivation of high and low pathogenic avian influenza virus H5 subtypes by
521 copper ions incorporated in zeolite-textile materials. Antiviral Res 93:225-233.

522 27. Binder H, Arnold K, Ulrich AS, Zschornig O. 2001. Interaction of Zn2+ with
523 phospholipid membranes. Biophys Chem 90:57-74.
524 28. Lindsley WG, Noti JD, Blachere FM, Thewlis RE, Martin SB, Othumpangat S,
525 Noorbakhsh B, Goldsmith WT, Vishnu A, Palmer JE, Clark KE, Beezhold DH. 2015.
526 Viable influenza A virus in airborne particles from human coughs. J Occup Environ
527 Hyg 12:107-13.
528 29. Cruz J, Leitao AC, Silveira D, Pichandi S, Pinto M, Fangueiro R. 2017. Study of
529 moisture absorption characteristics of cotton terry towel fabrics. Procedia
530 Engineering 200:389-398.
531 30. Erbil HY, Demirel AL, Avci Y, Mert O. 2003. Transformation of a simple plastic into a
532 superhydrophobic surface. Science 299:1377-80.
533 31. Borkow G, Zhou SS, Page T, Gabbay J. 2010. A novel anti-influenza copper oxide
534 containing respiratory face mask. PLoS One 5:e11295.
535 32. van Doremalen N, Bushmaker T, Morris DH, Holbrook MG, Gamble A, Williamson BN,
536 Tamin A, Harcourt JL, Thornburg NJ, Gerber SI, Lloyd-Smith JO, de Wit E, Munster VJ.
537 2020. Aerosol and Surface Stability of SARS-CoV-2 as Compared with SARS-CoV-1. N
538 Engl J Med 382:1564-1567.
539 33. Gandhi CS, Shuck K, Lear JD, Dieckmann GR, DeGrado WF, Lamb RA, Pinto LH. 1999.
540 Cu(II) inhibition of the proton translocation machinery of the influenza A virus M2
541 protein. J Biol Chem 274:5474-82.
542 34. Okada A, Miura T, Takeuchi H. 2003. Zinc- and pH-dependent conformational
543 transition in a putative interdomain linker region of the influenza virus matrix
544 protein M1. Biochemistry 42:1978-84.

545 35. Fodor E, Devenish L, Engelhardt OG, Palese P, Brownlee GG, Garcia-Sastre A. 1999.
546 Rescue of Influenza A Virus from Recombinant DNA. Journal of Virology 73:9679-
547 9682.
548 36. Te Velthuis AJW, Long JC, Bauer DLV, Fan RLY, Yen HL, Sharps J, Siegers JY, Killip MJ,
549 French H, Oliva-Martin MJ, Randall RE, de Wit E, van Riel D, Poon LLM, Fodor E.
550 2018. Mini viral RNAs act as innate immune agonists during influenza virus infection.
551 Nat Microbiol 3:1234-1242.
552 37. Simoes AE, Pereira DM, Amaral JD, Nunes AF, Gomes SE, Rodrigues PM, Lo AC,
553 D'Hooge R, Steer CJ, Thibodeau SN, Borralho PM, Rodrigues CM. 2013. Efficient
554 recovery of proteins from multiple source samples after TRIzol((R)) or TRIzol((R))LS
555 RNA extraction and long-term storage. BMC Genomics 14:181.
556
557
558 **Figure legends**
559
560 **Figure 1. Absorption and release of IAV and SARS-CoV-2 from fabrics**. **A**) Photographs of
561 cotton control, PA66 and polypropylene fabric samples. **B**) Schematic of experimental
562 procedure for exposing and isolating RNA virus from fabrics. **C**) Analysis of virus medium
563 retention by fabrics per volume of input medium. Values were obtained by weighing each
564 fabric before and after addition of virus medium, and after removal of the virus medium. **D**)
565 Analysis of virus medium retention by fabrics normalized by dry weight of each fabric.
566 Values were obtained by weighing each fabric before and after addition of virus medium,
567 and after removal of the virus medium. **E**) Plaque assay of IAV present in virus medium
568 after removal of the medium from each fabric. **F**) Quantitation of the amount of virus

569 remaining on each fabric, normalized by the dry weight of each fabric. **G**) Effect of different
570 tween-80 concentrations on IAV plaque assay read-out. **H**) Effect of 0.05% tween-80 in PBS
571 on the amount of virus released from each fabric. **I**) Quantitation of IAV titers after
572 absorption of the virus to the fabrics and washing of the fabrics with PBS or PBS containing
573 different concentrations of tween-80. **J**) Quantitation of SARS-CoV-2 titers after absorption
574 of the virus to the fabrics and washing of the fabrics with PBS or PBS containing different
575 concentrations of tween-80. Error bars indicate standard deviation. Asterisk indicates p-
576 value, with * $p<0.05$, ** $p<0.005$, and ns $p>0.05$.
577
578
579 **Figure 2. IAV is inactivated by zinc ions**. **A**) Plaque assay showing the effect of different
580 zinc chloride and EDTA concentrations on IAV titers. **B**) Experimental approach for
581 inactivating IAV with zinc ions and neutralization of zinc ions using EDTA. **C**) Cytotoxicity
582 analysis of zinc chloride and EDTA in MDCK cells. **D**) IAV titers after exposure to zinc
583 chloride and neutralization with EDTA as measured on MDCK cells. **E**) Western blot IAV HA
584 and NP protein levels after exposure to zinc chloride and neutralization with EDTA. Upper
585 panel shows quantitation of western signal and middle panel the western signal as detected
586 with LI-COR. Bottom panel shows NA segment RT-qPCR analysis of IAV virus after
587 exposure to zinc chloride and neutralization with EDTA. Error bars represent standard
588 deviation. Asterisk indicates p-value, with * $p<0.05$, ** $p<0.005$, and ns $p>0.05$.
589
590
591 **Figure 3. Inactivation of IAV and SARS-CoV-2 on fabrics**. **A**) Schematic of testing
592 procedure for fabrics without or with embedded zinc oxide. **B**) IAV titer in input, or PA66

593 control or KF1 fabric eluates. **C**) SARS-CoV-2 titer in input, or PA66 control or KF1 fabric
594 eluates. One representative experiment is shown. **D**) Western blot analysis of IAV HA and
595 NP protein levels after exposure of IAV to the KF1 or control fabric. Both the virus that was
596 removed (eluate) from each fabric with PBSTE as well as the virus that remained on each
597 fabric was analyzed. **E**) Western blot analysis of SARS-CoV-2 S and N protein levels after
598 exposure of virus to the KF1 or control fabric. Both the virus that was removed (eluate) from
599 each fabric with PBSTE as well as the virus that remained on each fabric was analyzed. **F**)
600 Time course of IAV or SARS-CoV-2 titer reduction by the KF1 fabric minus the titer
601 reduction by the PA66 control without embedded zinc. One representative time course is
602 shown. Data were fit with logarithmic equation. **G**) Reduction rate of IAV or SARS-CoV-2
603 titer after exposure to KF1 fabric. Data points were obtained by from time courses
604 experiments in which we varied the viral load and subsequently estimated the maximum
605 reduction rate (exponential phase) for each time course. Reduction was normalized to
606 $pfu \cdot gram^{-1} \cdot min^{-1}$ using the dry fabric weight. IAV and SARS-CoV-2 data points were fit with
607 a linear line and no difference was observed between the two fits. R^2 for IAV fit is shown. **H**)
608 Zinc content in KG6 fabric after repeated washing according to the standardized home
609 laundry test protocol AATCC M6-2016. One representative experiment for one batch of
610 fabric is shown. **I**) Reduction rate of IAV titer after exposure to unwashed or washed KG6
611 fabric. Error bars represent standard deviation. Asterisk indicates p-value, with * $p<0.05$
612 and ns $p>0.05$.
613